Micromechanical fracture analysis of amylose

W. R. Even and S. H. Carr
Department of Materials Science and Engineering and Materials Research Center, Northwestern University, Evanston, Illinois 60201, USA
(Received 22 April 1977; revised 21 November 1977)

Amylose films were prepared with two distinctly different microstructures, and these specimens were subsequently tensile-tested at different levels of moisture content. Measurement of the strain energy release rate, G_I, was approached from three separate methods. Two of these methods, the J integral and stress intensity analyses, are based on bulk tensile properties. The third method involves direct calculation of the work expended in producing the microplastic zone at the crack tip. Birefringence measurements were used in mapping the magnitude and shape of the plastic zones. Although the semicrystalline material would not lend itself to the bulk tensile analyses, G_I values were obtained via the optical analysis. For disordered amylose, G_I values derived from this optical analysis were found to correlate with those obtained from bulk measurements, and the fracture toughness was found to be comparable to that of other engineering polymers. Surprisingly, moisture content within the range investigated herein has no great effect on the strain energy release rate. This insensitivity is attributed to active interaction between the absorbed water and amylose macromolecules.

INTRODUCTION

Fracture mechanisms operable in semicrystalline polymers, elastomers, or polymer glasses are known to differ greatly[1]. The source of variety in fracture behaviour can be divided into two broad categories. The first results from variations in the chemical composition of the macromolecules themselves. Fracture in polymers is affected not only by primary and secondary structure but also by ability of chains to associate with their neighbours. The second category results from the variety in physical testing techniques. The multiplicity of methods[1] employed today yields a wealth of data, but each of these procedures usually involves a specific set of temperatures, geometries, strain rates, and states of stress. In recent years, a number of 'material constants' which are independent of the testing technique have been proposed[2]. One such parameter, the strain energy release rate, can be used[3] to remove the variability in fracture behaviour due to testing method. This then allows differences in failure behaviour to be directly related to the polymer itself.

Many varieties of polymer chain composition manifest themselves as differences in physical microstructure of the polymer solid, and the failure mechanisms of necking, crazing, and void formation[4–6] all reflect microstructural sensitivities. Environmental agents such as temperature, solutes, or solvents are also known to affect the failure process itself[7,8]. This is usually the result of changes in energetics or kinetics of polymer chain relaxations. Changes in microstructure involving fracture are intrinsically related to bulk mechanical properties, and a study relating microstructure to strain energy release rate could yield added insight into these fracture mechanisms.

Such a study is best pursued with a material available in two distinctly different microstructures. Amylose, a naturally occurring polymer isolated from plant starches, was chosen as our working material. Although the ether linkages in amylose might impart substantial rotational freedom to these chains, the presence of glucose rings causes the chain backbone to be sterically limited in its free rotation. As a result, the macromolecule behaves in a stiff manner[9], requiring cooperative motions of the individual segments. Among the energetically more favourable conformations for amylose are helices[10] which are stabilized by intramolecular hydrogen bonding. Hydrogen bonding character also becomes important in solution, and in this case the polymer adopts various conformations which are dependent on the solvent[11]. In solutions where solvent can easily accommodate most bonding requirements, amylose behaves as a random coil, but other solvents tend to solvate amylose as a helix[12]. This helix frequently forms with small molecules such as water bound in the interior. In many ways, the solid state microstructures of amylose reflect the conformation of molecules in solution. This microstructure can range from glassy to semicrystalline. In particular, many crystal structures have been reported which are composed of ordered helices with bound solvent[13–15]. Water, whether absorbed from the surroundings or as a solvent, affects the microstructure of amylose. Raman spectroscopy studies[16] show that water can hydrogen bond in the centre of amylose helices, resulting in a more relaxed structure. Any absorption into such free volume sites has the potential of altering the mechanical properties of the solid. The specific thrust of this research is aimed toward improving the understanding of the effect of different microstructures and absorption of water on the mechanical properties of these solids. This paper focuses on micromechanics of amylose films because the behaviour at this size scale has considerable influence over final service performance.

EXPERIMENTAL

Amylose (Superlose®, Stein, Hall and Co., New York) was dissolved in aqueous 1 N NaOH producing solutions 10% amylose by wt. Solutions were cast with a 50 mil film clearance blade onto glass plates. Transparent, disordered amylose films were obtained simply by drying these solutions in a vacuum. Alternatively, molecularly ordered films

0032–3861/78/1905–0583 $02.00

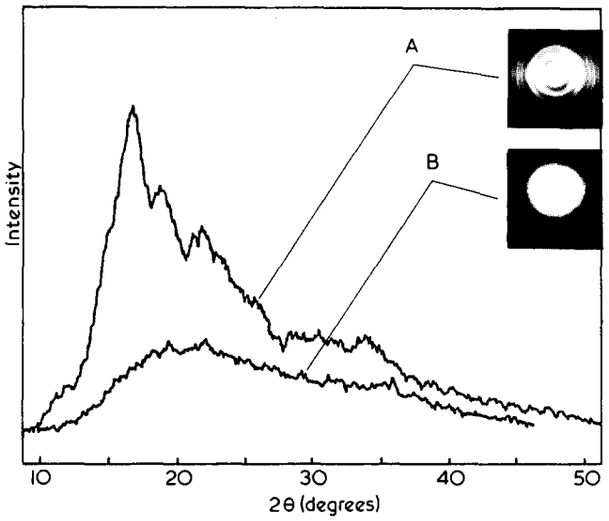

Figure 1 The difference in the microstructure of the two amylose-film preparations as demonstrated by X-ray diffraction. Comparison of the scattered intensity from both curves shows the semicrystalline material to be approximately 40% crystalline. A, semicrystalline; B, disordered

were obtained by causing wet solutions to gel by immersing them in ice–water. These solutions were sufficiently viscous to resist disruption during this process. After 30 min in this bath, the amylose was then converted into translucent, semicrystalline films by drying in a vacuum. No heating was involved in either the solution preparation or in the drying steps. Release of the finished 3 mil films was facilitated by a brief exposure to high humidity.

Tensile test specimens, 1.2 cm wide and 6 cm gauge length, were cut using a template and were subsequently pre-cracked via the following procedure. A notch was made with a scalpel in the specimen's edge near its midpoint. Specimens were mounted in a special fixture, and a crack was then propagated at liquid nitrogen temperatures by imposing a three-point bending stress locally about the tip of the notch. Some specimens were then transferred to a specially constructed tensile device sufficiently small to fit on the stage of an optical microscope. This specimen fixture was capable of humidity control within ±1% r.h. The microscope was fitted with crossed polarizers and a Berek (Leitz Co.) optical retardation compensator. It was then possible to observe cracks growing in areas whose surfaces had previously been marked with a vacuum-evaporated gold grid, 200 Å thick. Tensile testing was done at room temperature with an Instron testing machine at a strain rate of 0.04 min^{-1}. For each value of relative humidity, 20 specimens of varying crack length were tensile-tested. X-ray diffractometry was used to differentiate between different polymer microstructures. A Norelco diffractometer and cylindrical camera employing CuKα radiation were used in this work. The contrast in microstructure as revealed by X-rays is shown in *Figure 1*, where the semicrystalline material exhibits several local scattering maxima. Fracture surfaces were metallized *in vacuo* with gold and observed in a Kent–Cambridge S4 scanning electron microscope. Micrographs showed the pre-cracking method resulted in very sharp, brittle crack tips, with no residual plastic deformation apparent. No sign of crazing was observed in any of the fractured materials. Constant humidity atmospheres were obtained by bubbling air through saturated salt solutions, and the resulting equilibrium water content in amylose films is shown in *Table 1*. The films were observed to equilibrate within 24 h at room temperature, 23° ± 1°C.

RESULTS

The effect of water on mechanical properties of specimens was evident in handling the samples during preparation. In particular, disordered films behaved in a brittle manner at low humidities and became more ductile as humidity increased. Semicrystalline amylose seemed much less dependent on humidity. Bulk properties of both amylose preparations are given in *Table 2*. Note that the disordered material shows substantial modulus and fracture stress dependence on water content. This decrease in strength should be expected, since water is a swelling agent for amylose. Humidity data for semicrystalline material correlates well with the qualitative observations. By comparing the bulk X-ray scattering intensity for each amylose microstructure, the semicrystalline films were found to be approximately 40% crystalline. Three different techniques were used to measure material fracture parameters, as described below.

From the stress–strain curves, information can be obtained on the effect of specimen flaws. Stress intensifies locally at the crack tip and results in a plastic instability leading to premature failure. The resulting stress accumulation at a crack tip can be represented quantitatively by the stress intensity factor, K_I. Direct observation of fracture surfaces indicated that specimens failed primarily in simple tension, essentially on planes perpendicular to the tensile axis. The stress at which a material fails catastrophically, σ_f, reflects a critical stress intensity factor, K_{Ic}. The relationship between K_{Ic} and measurable bulk properties is shown below:

$$K_{Ic} = \sigma_f(\pi a)^{1/2} f(a/b) \quad (1)$$

where σ_f = ultimate fracture stress, a = crack length, b = specimen half-width, and $f(a/b)$ = correction for finite

Table 1 Equilibrium water content in amylose

R.h. (%)	Disordered (wt % water)	Semicrystalline (wt % water)
~0	2.0	2.4
23	6.4	7.9
39	11.4	10.6
58	19.3	14.2
78	~28	~17.5

Table 2 Tensile properties of unnotched amylose films

		Disordered†		Semicrystalline†	
R.h. (%)	Water (wt %)	$\bar{\sigma}_f$ (MN/m²)	$\bar{E}$ X 10^{-3} (MN/m²)	$\bar{\sigma}_f$ (MN/m²)	$\bar{E}$ X 10^{-3} (MN/m²)
~0	2.0	63.8 ± 1.9	6.49 ± 0.18		
	2.4			93.4 ± 3.3	2.82 ± 0.16
23	6.4	34.2 ± 0.3	1.63 ± 0.04		
39	11.4	34.4 ± 0.4	1.59 ± 0.03		
58	14.2			96.1 ± 2.2	3.83 ± 0.30
	19.3	32.1 ± 0.4	1.47 ± 0.02		
78	~28	30.0 ± 0.4	1.47 ± 0.02		

† Error represents one standard deviation in the mean

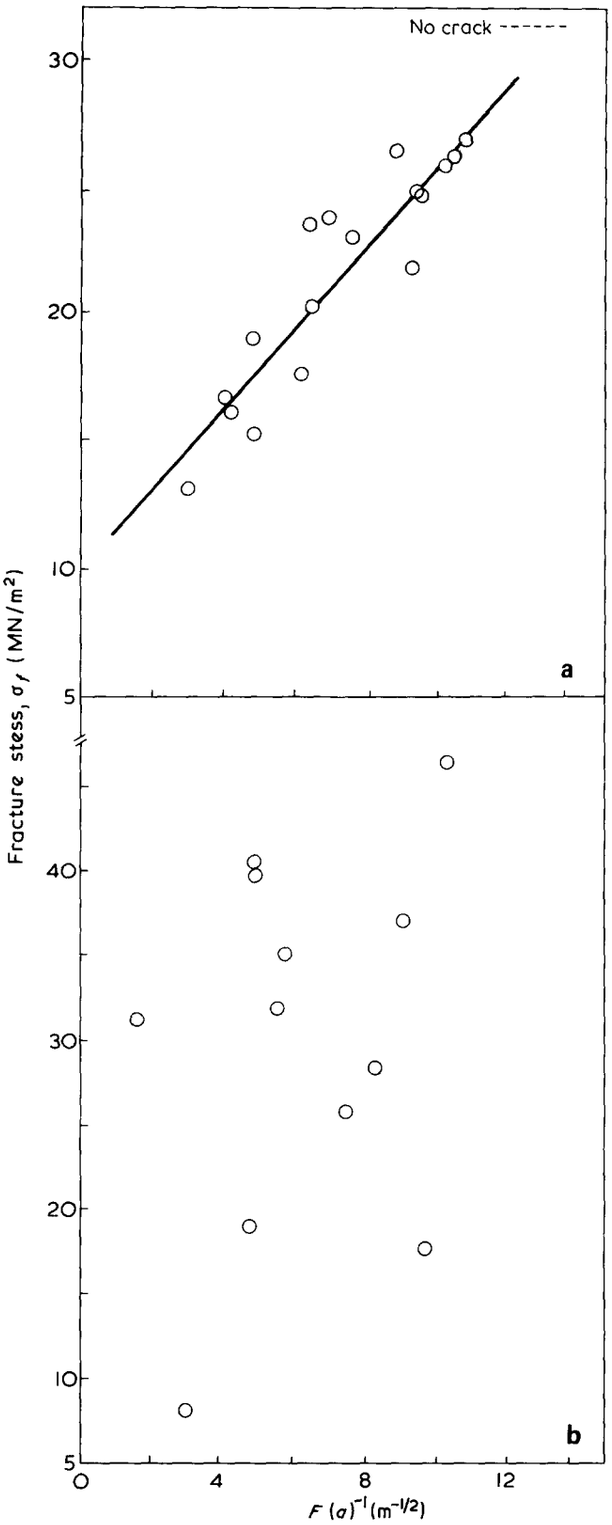

Figure 2 Stress intensity analysis for samples in equilibrium at 58% r.h., plotting ultimate fracture stress, σ_f, *versus* an inverse function of crack length. The disordered material (a) demonstrates an ability to conform to this analysis, while the semicrystalline (b) clearly does not

specimen size, due to Paris and Sih[17]. Equation (1) predicts a linear relationship between σ_f and $F(a)^{-1} = [(\pi a)^{1/2} f(a/b)]^{-1}$. An example of the data is shown in *Figure 2*. (This specific humidity reflects the maximum scatter experimentally observed.) From this Figure it can be seen that disordered material can be fitted by the stress intensity analysis, but the semicrystalline material yields results which cannot. This random pattern produced by the semicrystalline material is possibly the result of inhomogeneities within the material not apparent from casual inspection. Heterogeneities would be expected to affect the stress distribution locally about the crack tip; such random distortion of initial plastic zones could cause the observed erratic behaviour. Using the birefringence technique, this problem was averted because anomalous cracks could be rejected from the study.

The shape of a stress–strain curve is also sensitive to the presence of specimen flaws. Such sensitivity is thought to stem from changes in the stored energy within the test specimen. The J integral analysis[18] correlates changes in stored energy with the fracture toughness of a material. The J integral results from a summation of locally stored elastic energy along an arbitrary path passing through elastic material outside the plastic zone. This summation involves the difference between the stored strain energy and work needed to reduce traction forces on the crack surface to zero. As an alternative expression J_I is related to the potential energy, U', and its dependence on changes in crack length, a, is given in equation (2):

$$J_I = \int_\Gamma \left(W dy - \bar{T} \cdot \frac{\partial \bar{u}}{\partial x} ds \right) = -\frac{dU'}{da} \qquad (2)$$

where W = strain energy density; dy = an incremental displacement normal to the crack; $\bar{T}$ = traction vector on path Γ; $\bar{u}$ = the displacement vector; x = direction of crack propagation and ds = an incremental arc length along path Γ; Using the method described by Landes and Begley[19], the potential energy of the specimens was related to their respective crack lengths as shown in *Figure 3*. The method entails integrating the area beneath stress–strain curves, thus providing the energy involved. The lines represent the increased strain energy sensitivity of a fractured specimen at various total elongations. Qualitatively, this Figure is representative of data obtained at all the other humidities.

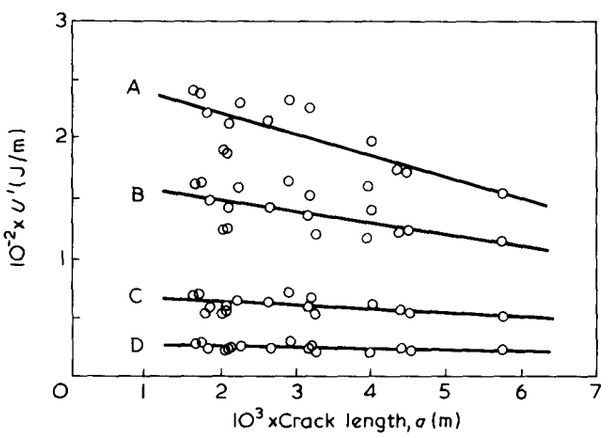

Figure 3 The stored potential energy, U', for a test specimen (58% r.h.) plotted against the crack length. The specimen elongation corresponds to the values shown in *Figure 7*. Disordered. Linear least squares value of the slopes taken at different total specimen elongation (x10^{-3}): A, 17.7; B, 9.5; C, 2.8; D, 0.85

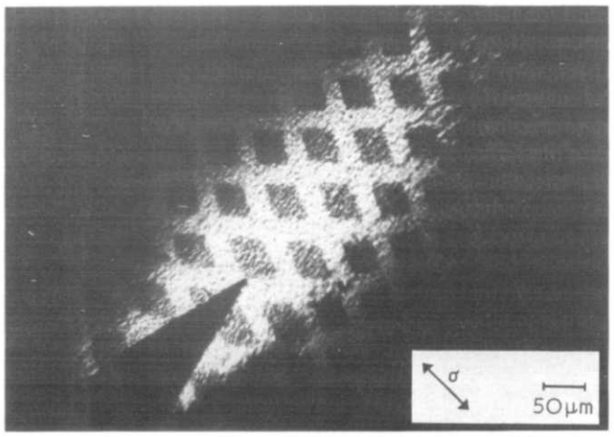

Figure 4 An optical micrograph of a semicrystalline specimen with a tensile stress perpendicular to the direction of crack propagation. Crossed polarizers reveal the strain field caused by the stress intensification around the crack tip. The textured appearance of the micrograph is due in part to scattering from small crystallites and mottling of the surface from stress.

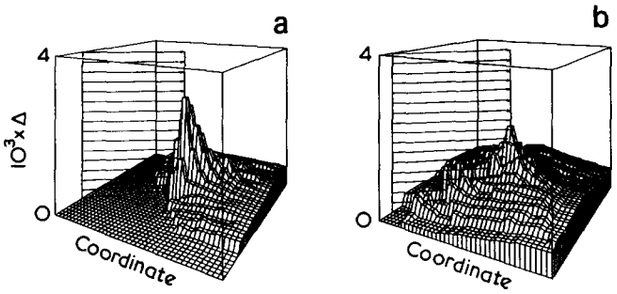

Figure 5 A map of experimental birefringence values, Δ, for both microstructures with reference to a coordinate system around the crack tip. The base of the cube represents an area 1 mm on a side. The arrows illustrate the plane of the crack, showing where the crack tip terminates. The length of the crack plane where non-zero birefringence values are observed represents the crack growth responsible for the observed strain field. (a) Disordered 58 r.h.; (b) crystalline 58 r.h.

The plastic instability which forms at a crack tip as the material is stressed produces local molecular orientation. Starting with either a disordered material or with randomly oriented crystallites, plastic yielding causes chain anisotropy, leading to bulk birefringence in the specimen. An optical micrograph of the strain field adjacent to a crack tip is shown in *Figure 4*. Three features stand out: (1) the open crack; (2) the shape and extent of the strain field; and (3) the gold reference grid. Some idea of the strain involved can be seen in the distortion of the reference grid. By using an optical retardation compensator and the coordinate system produced by the grid, a map of the relative change in birefringence was constructed. Examples of such birefringence maps are presented in *Figure 5*. As opposed to disordered amylose, where a rather featureless, symmetric birefringence zone is observed, the semicrystalline material has birefringence maxima at approximately 60° to the plane of the crack. Note that there is no difficulty in dealing with the semicrystalline amylose with this particular approach.

As has been emphasized earlier, the property of interest is the value of G_{Ic}, the critical strain energy release rate. This parameter is unique for a given material and represents the rate at which strain energy stored in the bulk can be relieved by advancement of a crack. This value is then characteristic of the fracture behaviour for amylose and, as in the treatment by Irwin[20], can be directly related to the critical stress intensity factor, K_{Ic}. In the case of thin films, the plane stress relationship between G_{Ic} and experimentally derived data is shown below:

$$G_{Ic} = \frac{K_{Ic}^2}{E} \tag{3}$$

where E is the bulk elastic modulus of the specimen. It is recognized that G_{Ic} values do vary[21] with specimen thickness for thin samples, but the extent to which this may affect data from the study reported here will need to await further experimentation. If a test specimen is sufficiently wide with respect to the crack length, then the J integral becomes identical to G_I. It is known that values of J_{Ic} seem to extrapolate toward typical G_{Ic} measurements. In our case, specific data for J_{Ic} values were not available.

It should be noted further that the J integral may not be strictly applicable to thin films – plane stress situations. Nevertheless, it has been asserted by Rice that 'the path-independent integral J is an effective tool for analysis in these [plane stress] cases'[22]. The thin film geometry was unavoidable because of the need to have precise control over moisture content and our inability to make thicker samples with uniform properties throughout. Strain energy release rates were derived using the measured values for K_{Ic} and E. These results are plotted in *Figure 6*. This plot represents the strain energy release rate at which unstable crack propagation occurs and its dependence upon water absorption.

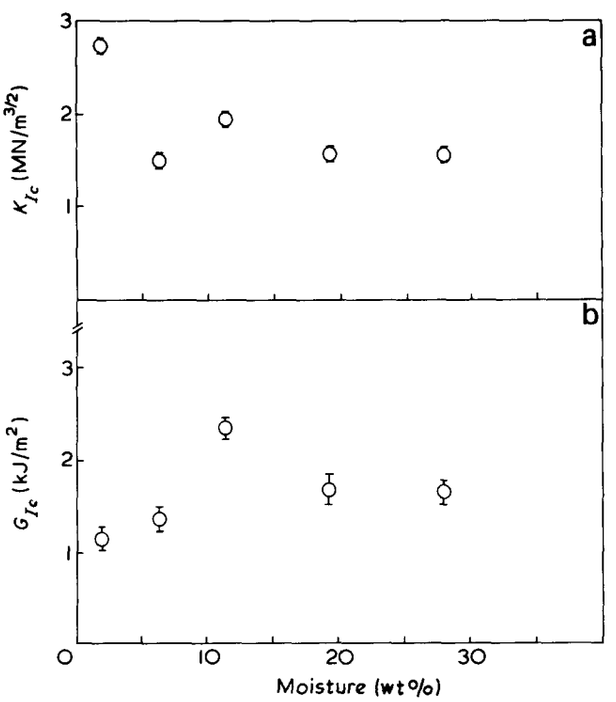

Figure 6 (a) The critical stress intensity factor, K_{Ic}, for disordered amylose films at various levels of moisture absorption. (b) The critical fracture toughness or strain energy release rate, G_{Ic}, as derived from equation (3). Note that there is a very mild dependence on moisture content

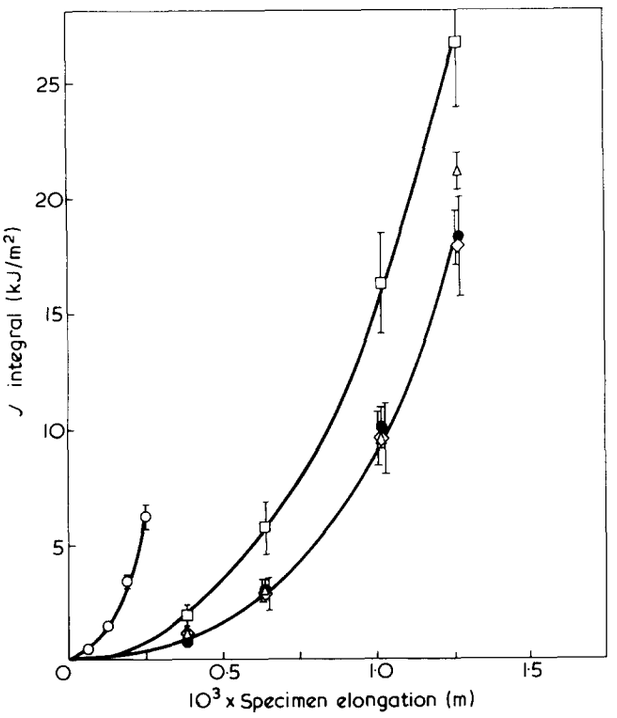

Figure 7 The *J* integral for disordered material and its dependence on both specimen elongation and moisture content. Within experimental error, three of the *J* integral curves are represented by a single line. Moisture (wt %): ○, 2.0; ●, 6.4; □, 11.4; ◇, 19.3; △, 28

The toughness derived from the *J* integral approach (see *Figure 7*) is shown as a function of total specimen elongation. In this Figure, the total toughness behaviour of the material is obtained rather than only the value at catastrophic failure. If information had been available for the exact displacement which resulted in unstable growth, a corroborating value of G_{Ic} could have been found. The agreement between our data and the *J* integral analysis lends credence to use of this technique on amylose with the specimen geometry used.

Correlating birefringence maps with the strain energy release rate is less rigorous but possibly more direct. Firstly, it requires that the molecular orientation producing birefringence be related to local strains. This was accomplished through point by point measuring of changes in the size of gold grids on the specimen surface. Independent thickness measurements support use of the approximation of constant volume, allowing 2-dimensional strain measurements from the surface to predict bulk strain. For birefringence and bulk strain measurements an experimental strain-optical coefficient was calculated, $2 \times 10^{-2}\ \Delta/\epsilon$. This allows the birefringence map to be transformed into its corresponding strain field. Secondly, stress was related to strain by a Dugdale-type model. The model assumed that stress rises monotonically with strain until the yield stress is reached and then remains constant at that level during yielding. Actual modulus and yield stress values were taken from measurements on bulk materials. The strain fields, in conjunction with the yielding model, now represent both stress and strain behaviour. Referring to *Figure 3* in the *J* integral analysis, energy per unit thickness can be calculated directly from the microstress–strain behaviour. Integrating the product of stress and strain [$(\sigma\epsilon)$/unit area] over the whole strain field results in the accumulated deformation energy, U'. *Figure 5* thus quantitatively describes the energy distribution around the crack tip. Because the value of the *J* integral, dU'/da, can be replaced by finite differences, $\Delta U'/\Delta a$, and because the length of crack responsible for a given $\Delta U'$ is known, fracture toughness can then be derived from micromechanical birefringence experiments. Strain energy release rate values resulting from combined optical measurements and the presumed stress–strain model are found to be within a factor of three larger than G_{Ic} values obtained from the stress intensity analysis. Fracture toughness measurements obtained by optical methods for the semicrystalline material were not experimentally distinguishable from the toughness of disordered amylose at each value of humidity. This may indicate that the approximately 60% disordered material in semicrystalline amylose is responsible for the major contribution to toughness measurements.

DISCUSSION

Both stress intensity and *J* integral analyses are macroscopic tests, in that they relate to experimental quantities averaged over numerous specimens. This averaging is, in general, an advantage, since small inhomogeneities associated with any specific sample are lost. If, however, these inhomogeneities are large, the range of test results may be so broad that correlation of separate results into a single relationship like the *J* integral becomes impossible. This may be the case with respect to crystalline amylose, although low levels of ductility at distances removed from the plastic zone may have resulted in scatter sufficient to preclude an analysis like either the *J* integral or stress intensity relationship requires. As a contrast to these macroscopic techniques, optical analysis, a microscopic technique, permits direct observation of the plastic zone and therefore visual discrimination of specimens with or without inhomogeneities affecting their crack tips.

In comparison with stress intensity values, the toughness derived from optical measurements was expected to be larger, due to an elastic birefringence contribution. An elastic stress was maintained across the samples to prevent residual plastic stresses from distorting the specimens and introducing thickness artefacts. With sufficiently small strains, the elastic contribution could be measured and the correction applied to the optical data. It is not yet clear whether the elastic contribution is solely responsible for the systematic difference between the optical data and data obtained from bulk measurements. Refinements in the optical technique may yield a powerful tool for quantitative study in fracture. Measurements associated with molecular orientation correspond closely to the micromechanical processes involved at the crack tip. Optical analysis made possible by transparent polymers provides detailed information for theoretical model predictions of plastic zone size, shape, and growth rate.

The rather mild humidity dependence observed in the amylose fracture toughness is surprising. The original solvent for film preparation was an aqueous alkaline solution. Since some sodium hydroxide remains in dried films, the absorption of moisture seems likely to result in a resolvation of the amylose chains; consequently, one might expect that the mechanical properties would deteriorate drastically when sorbed water levels reach 28 wt %. Yet the toughness or energy required to advance a crack is rather

insensitive to increased incorporation of water! The retained toughness may possibly be explained by water being incorporated into a 'structurally active' state, i.e. intra- and intermolecular hydrogen bonding. This would initially offset the capacity of water to disrupt molecular organization by solvation. It is interesting to note that the semicrystalline amylose actually exhibits an increased modulus due to water absorption. One explanation for the unique hydration properties of saccharides[23] is the geometrical arrangement of the hydroxyl groups. This arrangement allows saccharides to participate in the tridymite structure of water at room temperature. The binding[24] of water is a well documented phenomenon in many biopolymers. In particular, cellulose, which has the identical chemical composition as amylose, demonstrates[25] that water can participate in several distinct levels of binding. This type of participation would lend support to the hypothesis that absorbed water performs a structurally active role by hydrogen bonding between amylose molecules and increasing the energy required to advance a crack.

The peak in fracture toughness observed in *Figure 6* is of particular interest. Johnson and Radon[26] found toughness peaks in poly(vinyl chloride) and were able to correlate those peaks with mechanical relaxation processes. They attributed the increase in toughness to increased energy dissipation at the crack tip resulting from relaxation mechanisms at the test temperature. The possibility of correlation with mechanical relaxation processes leads to speculation that the absorbed water in amylose may contribute to a mechanically active loss process. Bradley and Carr[27] reported observing relaxation processes which were attributed to water–amylose complexes. We proposed that the small maximum in toughness seen in *Figure 6* may be due to specific molecular binding by water, a mechanically active loss process, or a combination of both. Clearly, the trend toward increasing toughness which we observe cannot continue indefinitely but must drastically decrease as water eventually replaces all interamylose hydrogen bonds.

CONCLUSIONS

Fracture processes in amylose films were characterized by both a procedure based on measurement of the microplastic zone and an analysis based on determination of bulk properties. Direct observation of crack tips reveals a birefringence pattern which has been shown to correlate with the strain field in the bulk that forms in advance of a propagating crack. This birefringence pattern provides information on size and shape of the microplastic zone, and it enables calculation of work needed to form such zones. The strain energy release rate derived from optical analysis of these plastic zones is comparable with values obtained from either the J integral or stress intensity analysis. Interestingly, the incorporation of increasingly higher amounts of water does not greatly affect the energy required to advance a crack through an amylose specimen.

ACKNOWLEDGEMENTS

The generous support of the National Science Foundation through grant ENG 74–18131 is gratefully acknowledged.

REFERENCES

1 Vincent, P. I. in 'Encyclopedia of Polymer Science and Technology', Wiley, New York, 1967, Vol. 7, p.292
2 Knott, J. F. in 'Fundamentals of Fracture Mechanics', Butterworth, London, 1973, Ch. 6, p.150
3 Begley, J. A. and Landes, J. D. in Proc. 1971 Nat. Symp. Fracture Mechanics, ASTM STP 514, American Society for Testing and Materials, 1972, Part 2, p.1
4 Vincent, P. I. in 'Proc. Conf. for the Physical Basis of Yield and Fracture', Institute of Physics and the Physical Society, London, 1966, p.155
5 Beaham, P., Bevis, M. and Hull, D. *Phil. Mag.* 1971, **24**, 1267
6 Hull, D. and Owens, T. W. *J. Polym. Sci. (Polym. Physics Edn)* 1973, **11**, 2039
7 Kambour, R. P., Romagosa, E. E. and Gruner, G. L. *Macromolecules* 1972, **5**, 335
8 Brown, W. *J. Polym. Sci. (Polym. Phys. Edn)* 1973, **11**, 2099
9 Carr, S. H., in 'First Cleveland Macromolecular Symp. Proc.', Elsevier, Netherlands, 1977, p.203
10 French, A. D. and Murphy, V. G. *Carbohydr. Res.* 1973, **27**, 391
11 Senior, M. B. and Hamori, E. *Biopolymers* 1973, **12**, 65
12 Banks, W. and Greenwood, C. T. *Biopolymers* 1972, **11**, 315
13 Valletta, R. M., Germino, F. J., Lang, R. E. and Woshy, R. J. *J. Polym. Sci. (A)* 1964, **2**, 1085
14 Zaslow, B., Murphy, V. G. and French, A. D. *Biopolymers* 1974, **13**, 779
15 Blackwell, J., Sarko, A. and Marchessault, R. H. *J. Mol. Biol.* 1969, **42**, 379
16 Cael, J. J., Koenig, J. L. and Blackwell, J. *Carbohydr. Res.* 1973, **29**, 123
17 Paris, P. C. and Sih, G. C. in 'Progress in Flaw Growth and Fracture Toughness Testing,' ASTM STP 381, American Society for Testing and Materials, 1965, p.30
18 Rice, J. R. *J. Appl. Mech. Trans.* 1968, **35**, 379
19 Landes, J. D. and Begley, J. A. in 'Proc. 1971 Nat. Symp. Fracture Mechanics', ASTM STP 514, American Society for Testing and Materials, 1972, Part 2, p.24
20 Knott, J. F. in 'Fundamentals of Fracture Mechanics', Butterworth, London, 1973, Ch 4, p.106
21 Tetelman, A. S. and McEvily Jr, A. J. in 'Fracture of Structural Materials', Wiley, New York, 1967, p.132
22 Rice, J. R. in 'Fracture, An Advanced Treatise', (Ed. H. Liebowitz), Academic Press, New York, 1968, Vol 2, pp.262–264
23 Franks, F. A. in 'Water, A Comprehensive Treatise', Plenum Press, New York, 1975, Vol. 4, p.519
24 Watt, I. C. and D'Arcy, R. L. *J. Polym. Sci. (Polym. Symp.)* 1976, **55**, 155
25 Nelson, R. A. *J. Appl. Polym. Sci.* 1977, **21**, 645
26 Johnson, F. A. and Radon, J. C. *J. Polym. Sci. (Polym. Chem. Edn)* 1975, **13**, 495
27 Bradley, S. A. and Carr, S. H. *J. Polym. Sci. (Polym. Phys. Edn)* 1976, **14**, 111